Turkish Online Journal of Qualitative Inquiry (TOJQI)
Volume 11, Issue 4, December 2020: 1979 - 1990

Review Article

Investigation Of the Physico-Chemical Characterization OF $Alpo_4$ Based Molecular Sieves

Dr. Neelu Jain[1], Rajeev Kumar Jha[2]

[1] Research Guide, Department of Chemistry, Sri Satya Sai University of Technology & Medical Sciences, Sehore, M.P.
[2] Research Scholar, Department of Chemistry, Sri Satya Sai University of Technology & Medical Sciences, Sehore, M.P.

Abstract

Microporous aluminophosphate have aroused wide interest because of their rich structural chemistry and potential applications in catalysis and adsorption. In recent years, the mesoporous aluminophosphate and metal ion substituted AlPO4 based materials are well known for their applications as heterogeneous catalysts. The synthesized materials are characterized before to apply as adsorbents for the removal of organic dyes from aqueous solution. In this investigation, the characterization techniques such as FT-IR, XRD, N_2 sorption analysis, TGA and SEM are carried out to confirm the formation of aluminophosphate tetrahedral framework, crystalline nature, surface area, pore diameter, thermal stability and morphology respectively.

Keywords: Characterization, Aluminophosphate, Thermal stability, Morphology

Introduction:

The synthesis of aluminophosphate based materials (AlPO4, Zn-AlPO4, Fe-AlPO4 and Mg-AlPO4) are characterized before to apply as adsorbents for the removal of organic dyes from aqueous solution. In this investigation, the characterisation techniques such as FT-IR, XRD, N_2 sorption analysis, TGA and SEM are carried out to confirm the formation of aluminophosphate tetrahedral framework, crystalline nature, surface area, pore diameter, thermal stability and morphology respectively.

a. Fourier transform Infrared spectroscopy

The infrared spectrum of absorption or emission of a solid, liquid, or gas is obtained using the Fourier transform infrared spectroscopy (FTIR) technique. An FTIR spectrometer obtains high-resolution spectral data over a large spectral range at the same time.

In this technique, about 15 mg of finely powdered sample was well mixed with 200 mg of KBr powder. The pellet was prepared by the pressurized sample under the pressure of 5 tones. The sample pellet was fixed with FT-IR sample holder and it was immediately placed in the FT-IR instrument for analysis from the wavenumber 4000 to 400 cm^{-1}.

b. Powder X-ray diffraction

X-ray powder diffraction (XRD) is a rapid analytical technique primarily used for phase identification of a crystalline material and can provide information on unit cell dimensions. The analyzed material is finely ground, homogenized, and average bulk composition is determined.

X-ray diffraction (XRD) patterns at low angle were recorded on a Simanzu 6000 diffractometer using Cu-Ka radiation (1 = 1.5406 A) with a voltage 30 kV and current 30mA at room temperature with the scanning rate of 0.5 degree per minute.

c. N_2 sorption analysis

The nitrogen adsorption method can be used to investigate the concentration analysis of pore structures with lower pore sizes, as well as the accurate analysis of material mesopores and macropores. Nitrogen adsorption - desorption measurements were made by using Micromeritics, ASAP 2020 V3.00 H at 77K. The surface areas of the samples were obtained by the Brunauer-Emmett-Teller (BET) method and the pore size distribution was calculated by BJH (Barrett-Joyner-Halenda) method.

d. Thermal analysis

Thermal analysis is a broad phrase that refers to a technique for determining the time and temperature at which physical changes in a substance occur when it is heated or cooled. Each technique is defined by the types of physical changes that are being investigated.

The thermal analysis of the $AlPO_4$ based samples were recorded by Thermogravimetric analysis on SDT Q600 V8.3 Build 101 at a heating rate of 20^oC/min.

e. SEM

The incident electron beam sweeps across the sample surface and interacts with the sample, generating backscattered and secondary electrons that are used to build an image of the sample.The morphology of the $AlPO_4$ was found by using scanning electron microscope analysis. The SEM images were recorded by Leo series VP1430 microscope, operated at 20kV.

A scanning electron microscope (SEM) with a resolution of 2 nm is used to analyse the topography of materials. An electron probe is scanned across the material's surface, and the electrons interact with it. Secondary electrons are emitted and recorded from the specimen's surface.

Methods [1-11]:

FT-IR

The Fourier transform Infrared (FT-IR) spectrums of the thermally treated or calcinated samples of mesoporous $AlPO_4$, Zn-$AlPO_4$, Fe-$AlPO_4$ and Mg-$AlPO_4$ are shown in Figure 1, Figure 2, Figure 3 and Figure 4 respectively. In the FT-IR spectrum of $AlPO_4$, the asymmetric stretching of tetrahedral $AlPO_4$ is observed near 1106 cm^{-1} and corresponding symmetric stretching is observed around 674 cm^{-1}. The bending mode is positioned near 466 cm^{-1}. These stretchings are corresponds to the tetrahedral framework of $AlPO_4$. The characteristic FT-IR peaks for aluminophosphate at 1106 cm^{-1}, 674 cm^{-1} and 466 cm^{-1} are shifted at lower wave number and the peaks appeared at 1100 cm^{-1}, 668 $cm^{-1}$and 450 cm^{-1} for mesoporous Zn-$AlPO_4$. It confirmed that the presence of Zn into the tetrahedral frame work of $AlPO_4$.

The asymmetric stretching of tetrahedral Fe-$AlPO_4$ is observed at 1100 cm^{-1} and corresponding symmetric stretching is observed around 670 cm^{-1}. The bending mode is positioned near 460 cm^{-1}. The FT-IR stretchings of Fe-$AlPO_4$ are shifted to lower wavenumber region compared to AlPO4. This may be due to the isomorphous substitution of Fe into the tetrahedral frame work of $AlPO_4$. The characteristic FT-IR peaks for aluminophosphate at 1106 cm^{-1}, 674 cm^{-1} and 466 cm^{-1} are shifted at lower wave number and the peaks are appeared at 1100 cm^{-1}, 672 cm^{-1} and 459 cm^{-1} for Mg-$AlPO_4$, It is an evidence for the presence of Mg into the tetrahedral framework of $AlPO_4$.

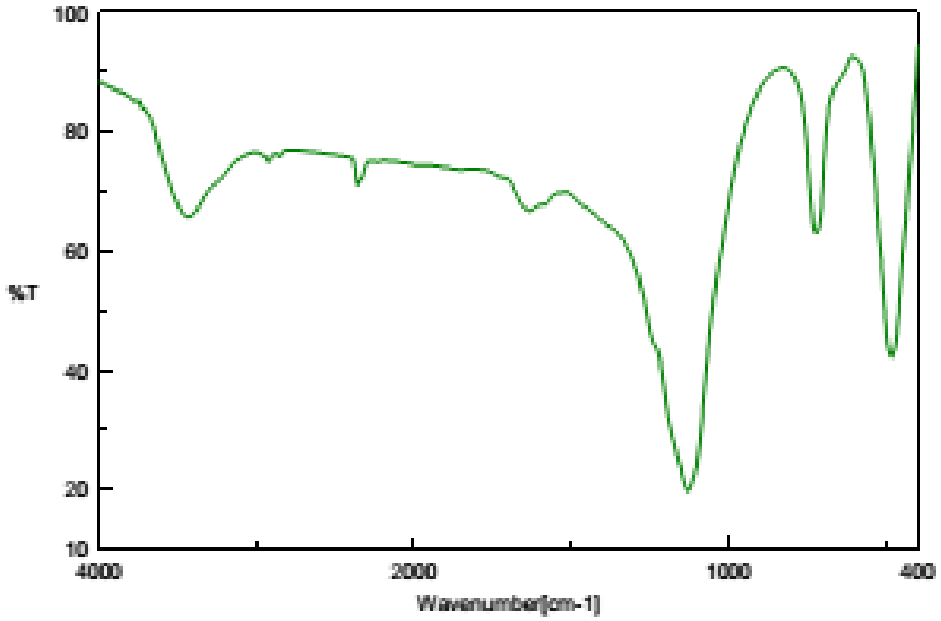

Fig 1: FT-IR spectrum of mesoporous $AlPO_4$

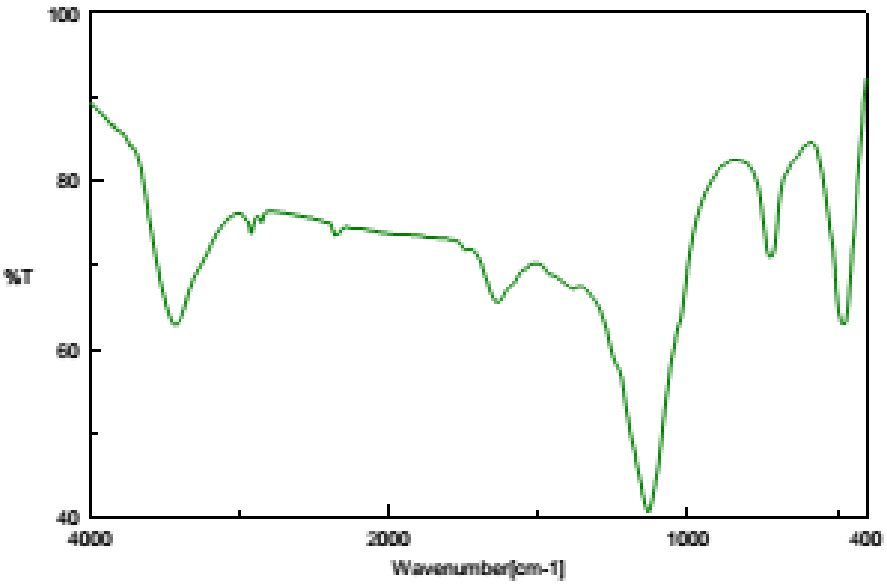

Fig 2: FT-IR spectrum of mesoporous Zn-$AlPO_4$

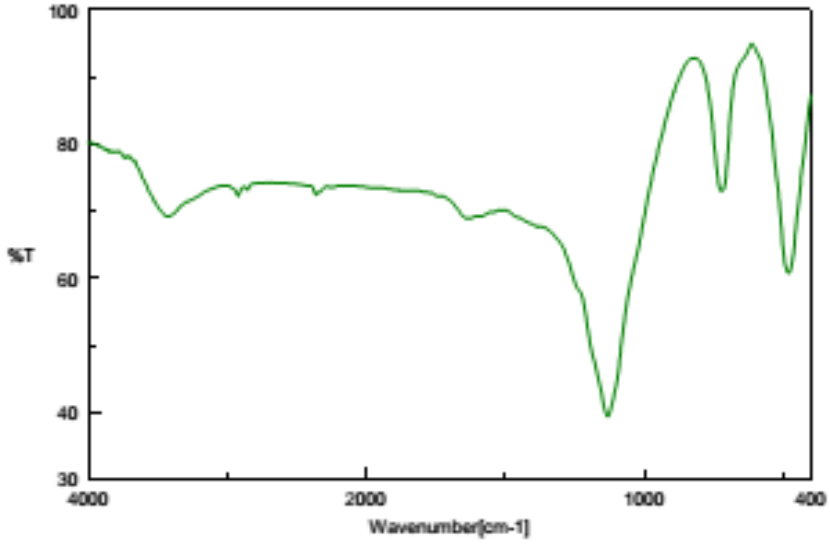

Fig. 3 : FT-IR spectrum of mesoporous Fe-$AlPO_4$

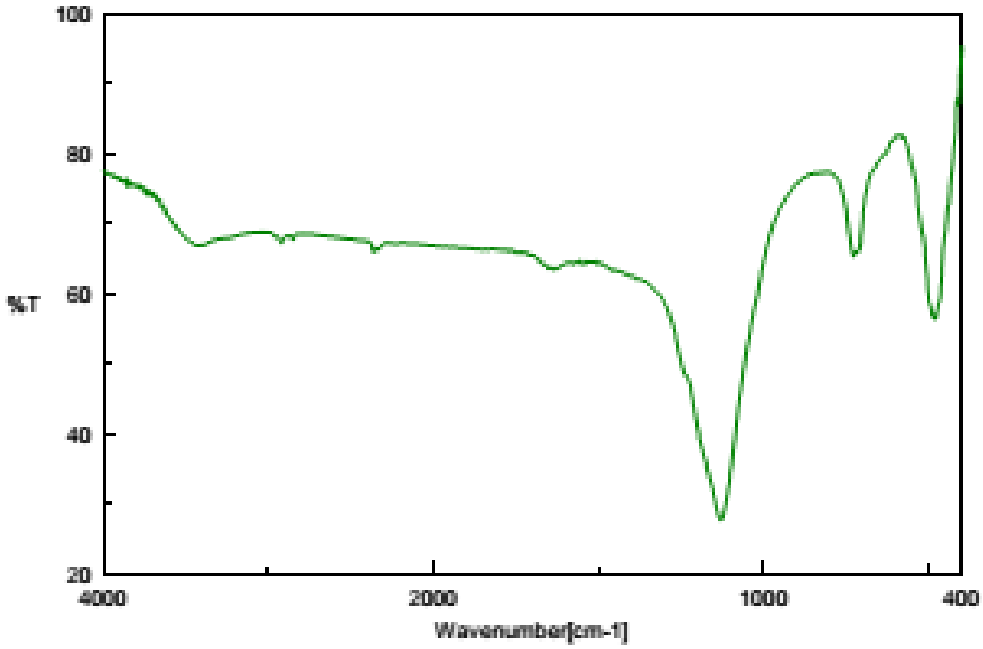

Fig. 4 : FT-IR spectrum of mesoporous Mg-$AlPO_4$

Powder X-Ray diffraction:

The powder X-ray diffraction pattern of calcinated mesoporous $AlPO_4$, Zn-$AlPO_4$, Fe-$AlPO_4$ and Mg-$AlPO_4$ are shown in Figure 5 - Figure 8. The XRD peak at low angle is typical for mesoporous materials.

In the XRD spectrum of mesoporous $AlPO_4$, a sharp peak around 1.2^o of the calcined sample interpreted that the high ordering of the material. The calcined material also indicates an additional peak at lower angles probably indicative of the presence of some dislocated crystals suggesting that some of the

ordering is destroyed by the high temperature calcination. The d spacing value at 73 A indicates the large pore of the $AlPO_4$.

A single XRD peak obtained for Zn-$AlPO_4$ at lower 20 value (1.6°) and at high d- spacing (80 A) than $AlPO_4$ (20 = 1.2°; d-spacing value = 73 A) confirm the incorporation of Zn^{2+} into the tetrahedral framework of AlPO4. In the XRD spectrum of mesoporous Fe- $AlPO_4$, a single peak is obtained at lower 20 value (1.1°) and at high d-spacing (82 A), which are higher than $AlPO_4$ (20 = 1.2°; d-spacing value = 73 A). This is may be due to the incorporation of Fe^{3+} into AlPO4 tetrahedral framework. The XRD pattern for Mg- $AlPO_4$ consists of relatively one reflection at low 29 value 1.14° with the d-spacing of about 78 A. XRD peak at lower 20 and at large d-spacing than $AlPO_4$ (20 = 1.2°; d- spacing value = 73 A) confirm the incorporation of Mg^{2+} into Mg-$AlPO_4$ tetrahedral framework.

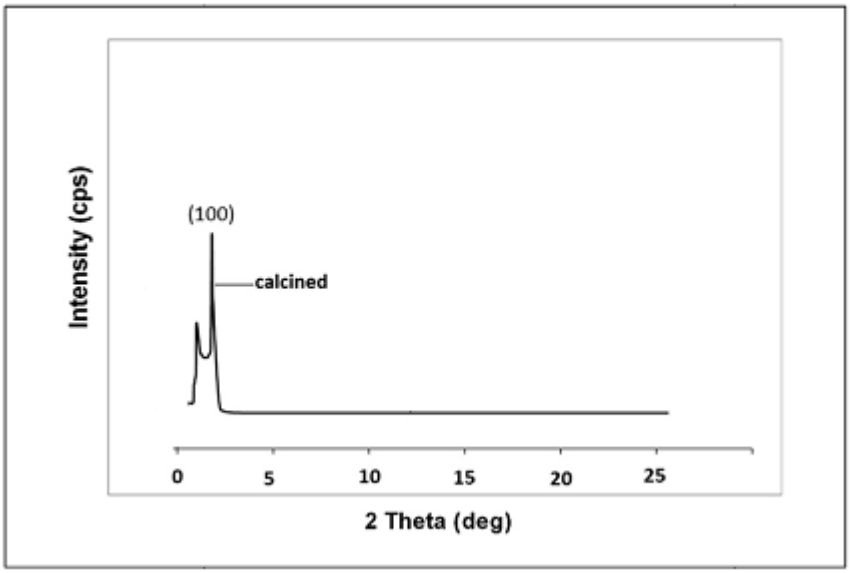

Fig: 5: Powder XRD spectrum of mesoporous $AlPO_4$

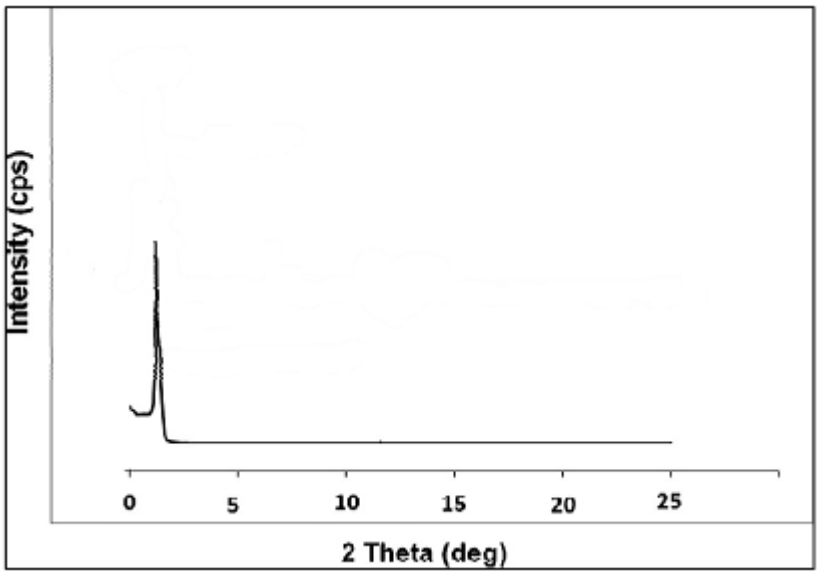

Fig:6: Powder XRD spectrum of mesoporous Zn-$AlPO_4$

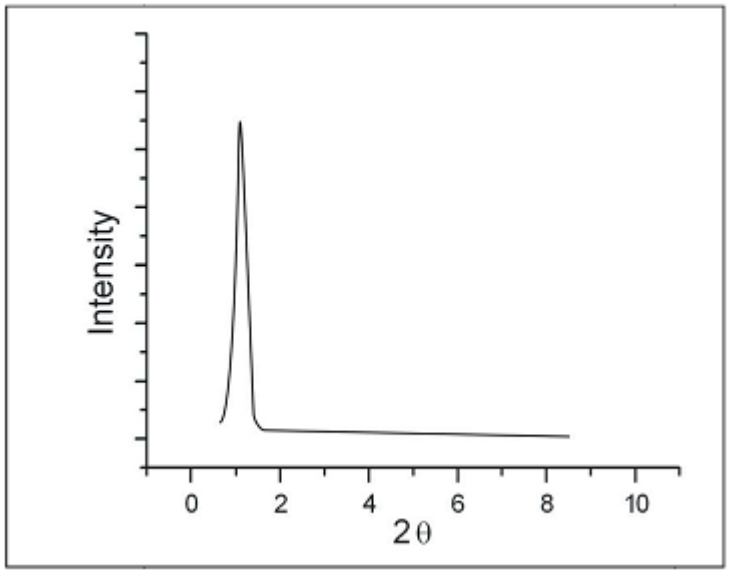

Fig: 7: Powder XRD spectrum of mesoporous Fe-$AlPO_4$

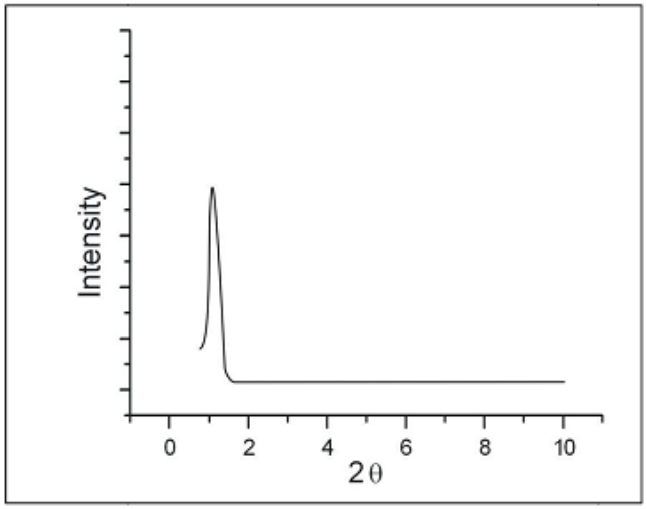

Fig: 8: Powder XRD spectrum of mesoporous Mg-$AlPO_4$

N_2 Adsorption- Desorption study:

Nitrogen sorption study gives detailed information of the material. The surface area and pore diameter are derived from the nitrogen sorption analysis. The isotherm plots and pore size distribution plots of mesoporous aluminophosphate based materials; $AlPO_4$, Zn-$AlPO_4$, Fe-$AlPO_4$ and Mg-$AlPO_4$ are shown in Figure 4.9, Figure 4.10, Figure 4.11 and Figure 4.12 respectively.

The pore volume, surface area and pore diameter of calcinated AlPO4 are 0.37cm^3/g, 97m^2/g and 15.3nm (153 A) respectively. N_2 adsorption at low relative pressure (P/P0 < 0.3) is accounted for monolayer adsorption of N_2 on the walls of the mesopores.

The pore diameter of mesoporous Zn-$AlPO_4$ is 22 nm (220 A) and the surface area is 80 m^2/g. The ionic radius of Zn^{2+} ion is 0.63A and the ionic radius of Al^{3+} ion is 0.53A. Zn has larger ionic radius than Al . Hence, the Zn-$AlPO_4$ has high pore diameter (22nm) than $AlPO_4$ (15.3nm). This confirms the incorporation of Zn into $AlPO_4$ tetrahedral framework. The Fe-$AlPO_4$ has 17nm (170 A) as pore diameter and 90 m^2/g as surface area. The ionic radius of Fe^{3}+ is 0.72A and the ionic radius of Al^{3}+ is 0.53A. Due to the large ionic radius of Fe^{3}+, The Fe-$AlPO_4$ has large pore diameter and low surface area than $AlPO_4$. This confirms the incorporation of Fe into Fe-$AlPO_4$ tetrahedral framework.

The pore size distribution (diameter) of Mg-$AlPO_4$ is maximum at 20nm (200 A) and the mesoporous Mg-$AlPO_4$ has the surface area 86 m /g. The ionic radius of Mg2+ ion is 0.72A and the ionic radius of Al^{3}+ ion is 0.53A. Due to the large ionic radius of Mg^{2}+, Mg-$AlPO_4$ has large pore diameter (20 nm) than the $AlPO_4$ (15.3 nm). This confirms the incorporation of Mg^{2+} into $AlPO_4$ tetrahedral framework.

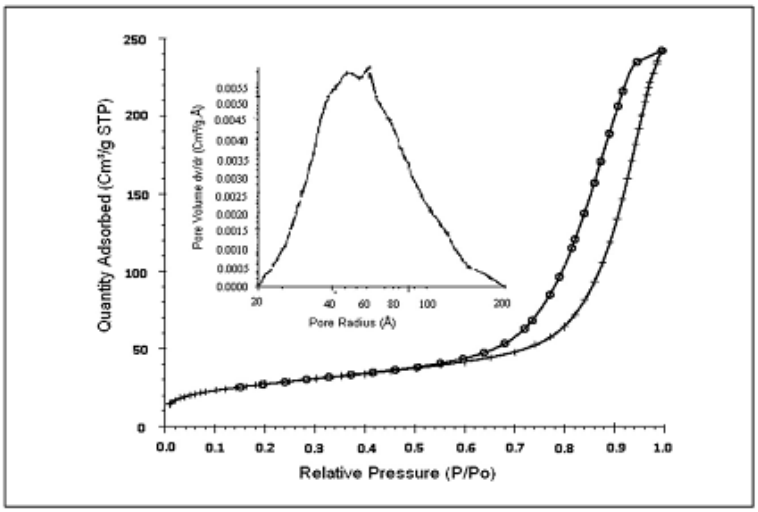

Fig:9: N2 sorption isotherm and pore distribution plot for mesoporous $AlPO_4$

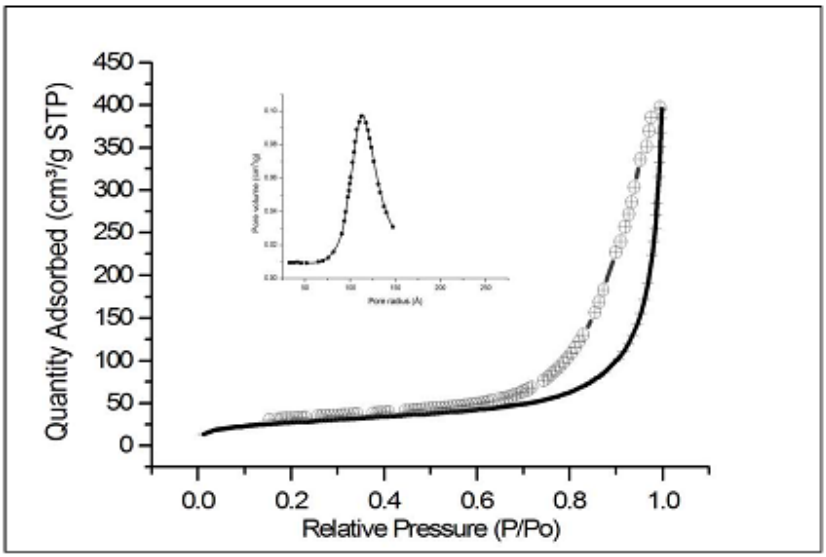

Fig: 10: N2 sorption isotherm and pore distribution plot for mesoporous Zn-$AlPO_4$

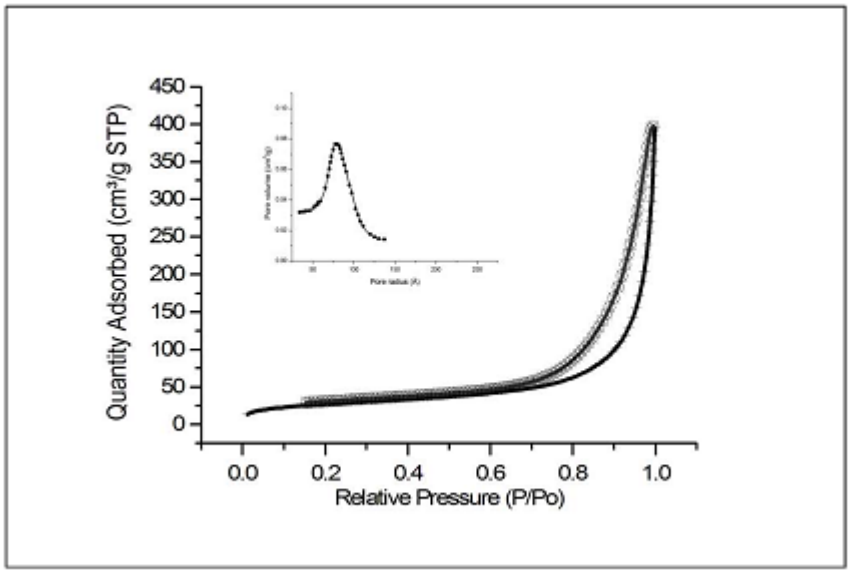

Fig: 11: N2 sorption isotherm and pore distribution plot for mesoporous Fe-$AlPO_4$

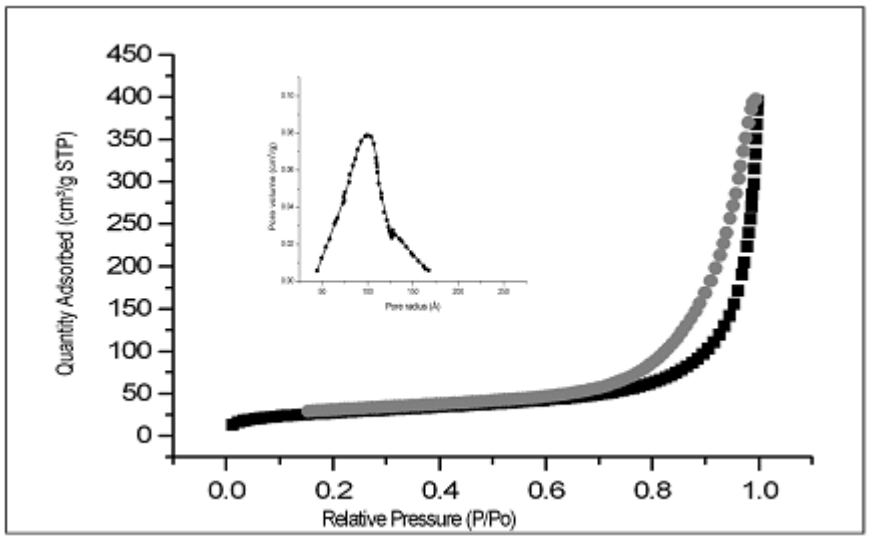

Fig: 12: N2 sorption isotherm and pore distribution plot for mesoporous Mg-$AlPO_4$

Thermal analysis:

The thermo gravimetric analysis of mesoporous aluminophosphate based materials ($AlPO_4$, Zn-$AlPO_4$, Fe-$AlPO_4$, and Mg-$AlPO_4$) gives the information about the thermal stability of the materials.

The thermograms for mesoporous $AlPO_4$, Zn-$AlPO_4$, Fe-$AlPO_4$, and Mg-$AlPO_4$ are shown in Figure 13, Figure 14, Figure 15 and Figure 16 respectively. The thermal analysis of as-synthesized mesoporous $AlPO_4$ based materials are studied upto 1200^{o}C. The weight loss at 115^{o}C is due to desorption of adsorbed water. The weight loss at 285^{o}C is attributed to the decomposition of template molecules. It suggests that the template can be completely removed around at 300^{o}C. Further increase of temperature shows no weight loss. This suggests that the material is stable above 1000^{o}C.

The same trend is observed for other aluminophosphate base materials; Zn-AlPO4, Fe-AlPO4, and Mg-AlPO4. Hence it is concluded that the all mesoporous AlPO4 based materials have high thermal stability

above 1000^{o}C. However, the reported mesoporous materials are stable only up to 800^{o}C.

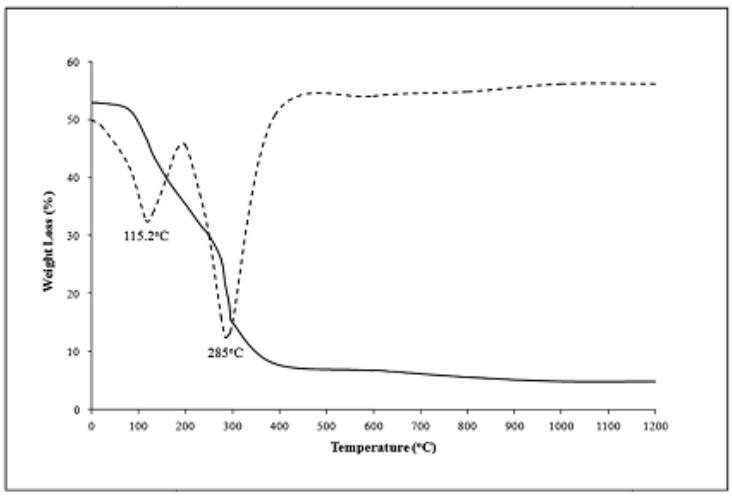

Fig: 13: Thermogram of mesoporous AlPO$_4$

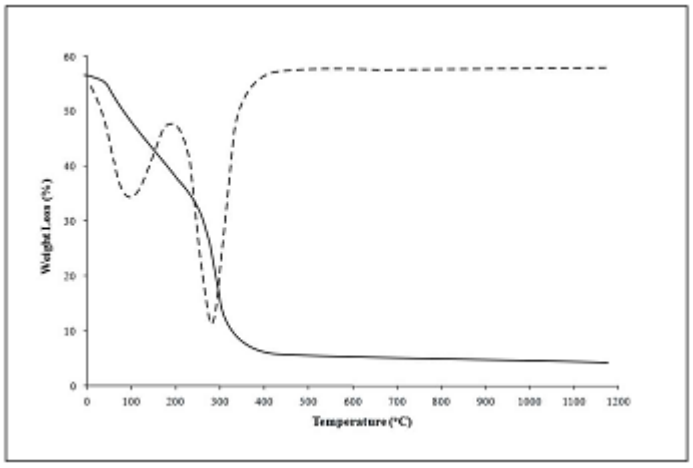

Fig. 14: Thermogram of mesoporous Zn-AlPO$_4$

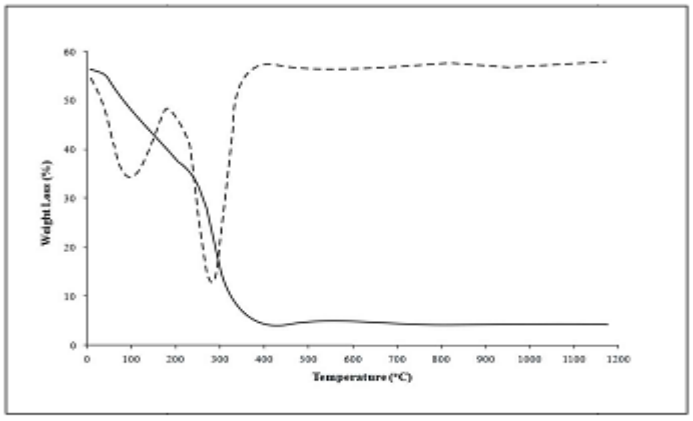

Fig: 15: Thermogram of mesoporous Fe-AlPO4

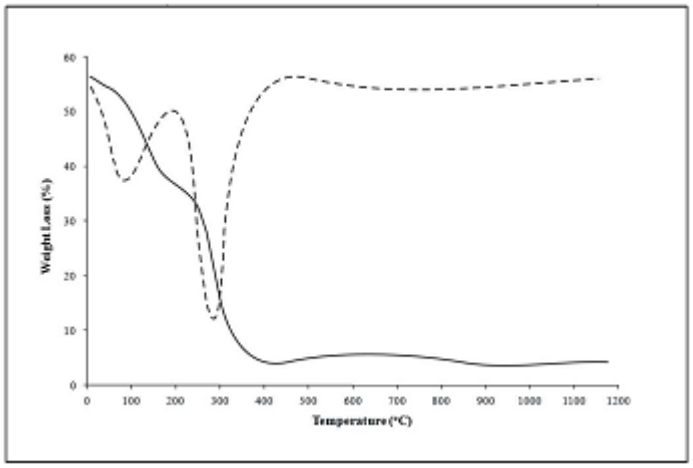

Fig:16: Thermogram of mesoporous Mg-AlPO4

SEM analysis

SEM images of calcinated $AlPO_4$, Zn-$AlPO_4$, Fe-$AlPO_4$ and Mg-$AlPO_4$ are shown in Figure 17, Figure 18, Figure 19 and Figure 20 respectively. The SEM image of the $AlPO_4$ sample show spherical morphology. It provides good evidence for crystalline nature of the aluminophosphate material. The morphology change indicates the incorporation of metal ions in the $AlPO_4$ based materials.

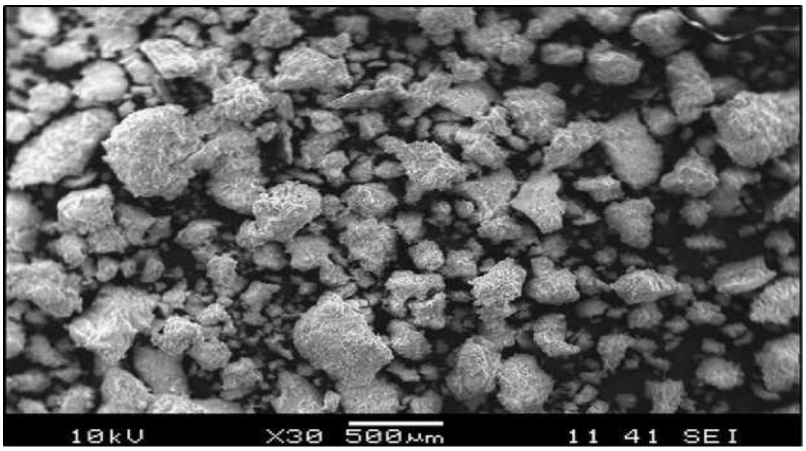

Figure 17 SEM image of mesoporous $AlPO_4$

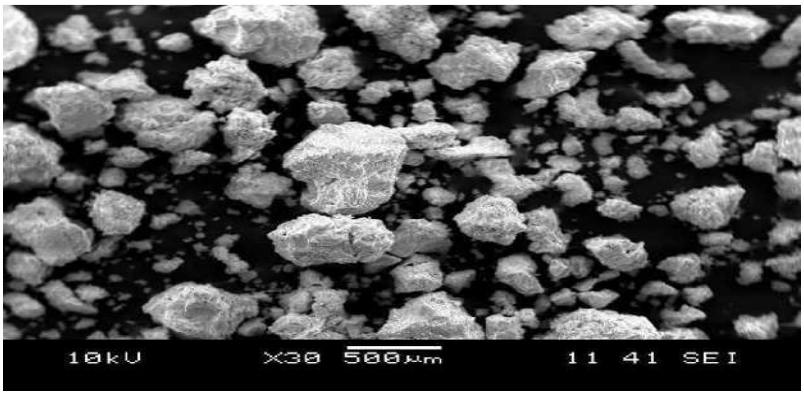

Figure 18 SEM image of mesoporous Zn-$AlPO_4$

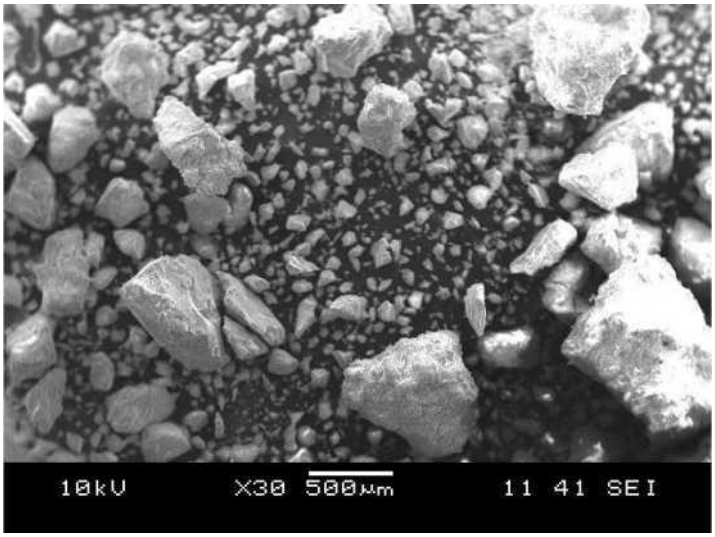

Figure 19: SEM image of mesoporous Fe-A1PQ_4

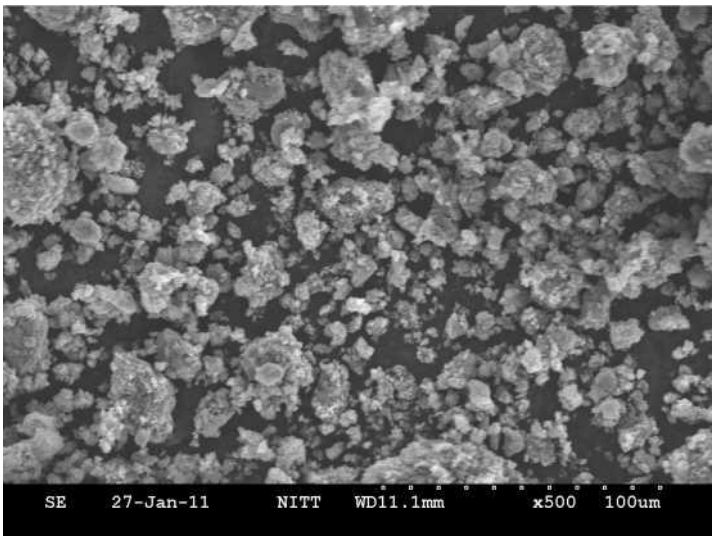

Figure 20 SEM image of mesoporous Mg-A1PO_4

CONCLISION:

The characterization data confirm that the well formation of mesoporous aluminophosphate based materials. These materials have high porosity (15-25nm) and high thermal stability (>1000^{o}C). The mesoporous aluminophosphate based materials have been used as adsorbents for the removal of cationic and anionic dyes.

REFERENCES:

1. Usha Nandhini K, Banumathi Arabindoo, Palanichamy M, Murugesan V, Journal of Molecular Catalysis A: Chemical, 223, 201-210 (2004).
2. N. Venkatathri, S.G. Hegde, V. Ramaswamy, S. Sivasanker, Microporous and mesoporous

materials, 23, 277-285 (1998).
3. Jian-Ming Lu, Koodali T. Ranjit, Pesak Rungrojchaipan, Larry Kevan, J. Phys. Chem. B., 109, 9284-9293 (2005).
4. O. Heloise Pastore, M. Munsignatti, R.S. Diomar Bittencourt, M. Ma'rcia Rippel, Micropor. Mesopor. Mater., 32, 211-228 (1999).
5. P. Selvam, S.K. Mohapatra, Journal of Catalysis, 238, 88-99 (2006).
6. Zhou Zhou, Gang Liu, Xiang Zhang, Xiang-Zhou Liao, Ya-Zhuo Hou, Ming-Jun Jia. Materials Letters 2005;59:3503-6.
7. Blacksmith Institute's The World's Worst Toxic Pollution Problems Report 2011, www.worstpolluted.org
8. Chellapandian Kannan, Thiravium Sundaram, Thayumanavan Palvannan, Journal of Hazardous Materials, 157, 137-145 (2008).
9. Jonathan Galownia, James Martin, Mark E. Davis, Microporous and Mesoporous Materials, 92 (1-3), 61-63 (2006).
10. Yasemin B, Haluk A, Desalination, 194, 259-267 (2006).
11. Mohamed Mokhtar Mohamed, Journal of colloid and interface science, 272, 28-34 (2004).